CHIN. PHYS. LETT. Vol. 38, No. 9 (2021) 097401 **Express Letter**

Observation of a Ubiquitous (π,π)-Type Nematic Superconducting Order in the Whole Superconducting Dome of Ultra-Thin $BaFe_{2-x}Ni_xAs_2$ Single Crystals

Yu Dong(董禹)[1,2,3†], Yangyang Lv(吕阳阳)[1,2,3†], Zuyu Xu(徐祖雨)[1,2,3†], M. Abdel-Hafiez[4,5], A. N. Vasiliev[4,6], Haipeng Zhu(朱海鹏)[7], Junfeng Wang(王俊峰)[7], Liang Li(李亮)[7], Wanghao Tian(田王昊)[1,2,3], Wei Chen(陈伟)[1,2,3], Song Bao(鲍嵩)[1,2,3], Jinghui Wang(王靖辉)[1,2,3,8], Yueshen Wu(吴越珅)[8], Yulong Huang(黄裕龙)[9], Shiliang Li(李世亮)[9], Jie Yuan(袁洁)[9], Kui Jin(金魁)[9], Labao Zhang(张蜡宝)[1], Huabing Wang(王华兵)[1], Shun-Li Yu(于顺利)[1,2,3*], Jinsheng Wen(温锦生)[1,2,3*], Jian-Xin Li(李建新)[1,2,3], Jun Li(李军)[8,1*], and Peiheng Wu(吴培亨)[1,10]

[1]*School of Electronic Science and Engineering & School of Physics, Nanjing University, Nanjing 210093, China*
[2]*National Laboratory of Solid State Microstructures, Nanjing University, Nanjing 210093, China*
[3]*Collaborative Innovation Center of Advanced Microstructures, Nanjing University, Nanjing 210093, China*
[4]*National University of Science and Technology (MISiS), Moscow 119049, Russia*
[5]*Department of Physics and Astronomy, Box 516, Uppsala University, Uppsala SE-75120, Sweden*
[6]*Moscow State University, Moscow 119991, Russia*
[7]*Wuhan National High Magnetic Field Center & School of Physics, Huazhong University of Science and Technology, Wuhan 430074, China*
[8]*ShanghaiTech Laboratory for Topological Physics & School of Physical Science and Technology, ShanghaiTech University, Shanghai 201210, China*
[9]*Beijing National Laboratory for Condensed Matter Physics & Institute of Physics, Chinese Academy of Sciences, Beijing 100190, China*
[10]*Synergetic Innovation Center in Quantum Information and Quantum Physics, University of Science and Technology of China, Hefei 230026, China*

(Received 1 August 2021; accepted 16 August 2021; published online 24 August 2021)

In iron-based superconductors, the $(0,\pi)$ or $(\pi,0)$ nematicity, which describes an electronic anisotropy with a four-fold symmetry breaking, is well established and believed to be important for understanding the superconducting mechanism. However, how exactly such a nematic order observed in the normal state can be related to the superconducting pairing is still elusive. Here, by performing angular-dependent in-plane magnetoresistivity using ultra-thin flakes in the steep superconducting transition region, we unveil a nematic superconducting order along the (π,π) direction in electron-doped $BaFe_{2-x}Ni_xAs_2$ from under-doped to heavily overdoped regimes with $x =$ 0.065–0.18. It shows superconducting gap maxima along the (π,π) direction rotated by 45° from the nematicity along $(0,\pi)$ or $(\pi,0)$ direction observed in the normal state. A similar (π,π)-type nematicity is also observed in the under-doped and optimally doped hole-type $Ba_{1-y}K_yFe_2As_2$, with $y = 0.2$–0.5. These results suggest that the (π,π) nematic superconducting order is a universal feature that needs to be taken into account in the superconducting pairing mechanism in iron-based superconductors.

DOI: 10.1088/0256-307X/38/9/097401

The high-temperature superconductivity in iron-based superconductors emerges from doping the parent compounds by either electrons or holes. In the typical 122-type iron-pnictides, their parent and under-doped samples undergo a structural transition from tetragonal to orthorhombic phases at the temperature T_s, followed by a magnetic ordering transition from paramagnetic to stripe antiferromagnetic (AFM) phases at T_N.[1–15] The structural transition breaks the four-fold (C_4) symmetry into a two-fold (C_2) one.[1–5] Intriguingly, despite the small difference of the lattice constants in order of ∼0.1% in the orthorhombic phase,[16–19] the antiferromagnetic order also exhibits a similar C_4-symmetry breaking, with moments ordered antiferromagnetically and ferromagnetically along the a and b axes (Fe–Fe bond directions), respectively, giving rise to a stripe antiferromagnetic order with an ordering wave vector of $(\pi,0)$.[1–15] Note that throughout the paper, we use the notation with one iron per

Supported by the National Natural Science Foundation of China (Grant Nos. 61771234, 61727805, 11674157, 11674158, 11774152, 11822405, 61521001, 61571219, and 61501222), the National Key Projects for Research and Development of China (Grant Nos. 2016YFA0300401, 2017YFB0503302, 2017YFA0304002, and 2017YFB0503300), the start-up funding from ShanghaiTech University, Innovative Research Team in University (PCSIRT), the Natural Science Foundation of Shanghai Municipality (Grant No. 20ZR1436100), the Science and Technology Commission of Shanghai Municipality (Grant No. YDZX20203100001438), Jiangsu Key Laboratory of Advanced Techniques for Manipulating Electromagnetic Waves, Natural Science Foundation of Jiangsu Province (Grant No. BK20180006), and the Fundamental Research Funds for the Central Universities (Grant No. 020414380117).
†These authors contributed equally to this work.
*Corresponding authors. Email: slyu@nju.edu.cn; jwen@nju.edu.cn; lijun3@shanghaitech.edu.cn
© 2021 Chinese Physical Society and IOP Publishing Ltd

unit cell. Electrical transport measurements further showed that the resistivity was larger along the slightly longer b-axis than that along the a-axis, which could extend to well above T_s.[17,19–25] Such an anisotropy between the a- and b-axes was subsequently observed by various techniques including quasi-particle-interference analysis from scanning tunneling microscopy,[16,18,26–29] angular-dependent nuclear magnetic resonance,[30–33] anisotropic spin excitations from neutron scattering,[34–38] band structure from angle-resolved photoemission spectroscopy,[39–43] and electronic Raman spectroscopy,[44–48] in almost all the iron-based systems. This anisotropic state is termed "nematic" phase, which is borrowed from a liquid-crystal phase to describe the electronic state breaking the rotational symmetry but preserving the translational symmetry.[49] Although the nematicity is believed to be of electronic origin,[49–59] the driving force for this nematic phase is still under debate, because the coupling of orbital and spin degrees of freedom makes it difficult to identify whether the spin or orbital fluctuations take the leading role.[29,32–34,39,40,44,49,54,60] Since the spin fluctuations favor a sign-changing s-wave superconducting state[61–64] ($s_{\pm}$) while the orbital fluctuations favor a sign-preserving s-wave state[65] (s_{++}), understanding the nematic phase can shed light on the superconducting mechanism in iron-based superconductors.[49,57,60] More importantly, given the universal presence of the electronic nematic phase and its proximity to the superconducting state, it is considered to have a close relationship with the superconductivity.[45,65–67] However, since such a nematic state was observed in the normal state, how it can be correlated with the superconducting state is still unclear.

In this respect, an important recent progress is that a nematic order was observed in an optimally doped hole-type $Ba_{0.5}K_{0.5}Fe_2As_2$ superconductor in the superconducting state.[68] It showed strong anisotropy in the in-plane magnetoresistivity on ultra-thin single crystals, which substantially enhanced the resistance and thus improved the sensitivity of the measurements.[68] Similar to that in the normal state, the nematicity is basically along the Fe–Fe bond direction (a or b-axis in the present design), which corresponds to $(0,\pi)$ or $(\pi,0)$ in the momentum space.[68] Since the sample was fabricated into a Corbino shape on an ultrathin crystal, the Lorentz force would not induce the anisotropic resistivity, and thus these results represent an intrinsic nematic superconducting state. Moreover, since both nematic phases in the normal and superconducting states were found in the similar concentrations, it was suggested that the nematic superconducting state may result from the normal-state nematic fluctuations typically surviving well above T_s.[22,49,54] Interestingly, in the heavily hole-doped $RbFe_2As_2$, whose doping concentration is far away from the nematic phase of the normal state in the phase diagram, a nematic superconducting state with a similar C_4-symmetry breaking but aligned along (π,π) (the Fe–As bond), was unveiled by the quasi-particle-interference measurement.[69] Furthermore, elastoresistance measurements in the normal state on this system also revealed a (π,π) nematicity.[70] The nematicity in the superconducting state provides a promising way to bridge the nematicity and superconducting pairing symmetry in iron-based superconductors. In particular, the (π,π) nematicity in superconducting states suggests that other collective fluctuations, different from the extensively studied stripe antiferromagnetic fluctuation, may also paly an important role in the superconducting mechanism, such as the double-stripe antiferromagnetic fluctuations[71,72] or other incommensurate collective fluctuations along the (π,π) direction. What is more, the collective fluctuations along the (π,π) direction could affect the gap symmetry and result in some complex gap structures.[73] Angle-resolved photoemission spectroscopy measurements on KFe_2As_2 have shown that the Fermi surfaces of the heavily hole-doped iron-based superconductors only have hole pockets centered at the Γ point without electron pockets at the M point.[73–75] This is very different from the under-doped and optimally doped samples where both electron and hole pockets are present.[1–5] Since the Fermi-surface topology is special in heavily hole-doped $RbFe_2As_2$, there appears a natural question whether such a (π,π)-type nematic order is unique for this doping or universal in the whole doping range.

In this work, by measuring the angular dependence of the in-plane magnetoresistivity in the whole superconducting dome of the electron-doped $BaFe_{2-x}Ni_xAs_2$ samples using ultra-thin flakes, we uncover a nematic superconducting order from under- to over-doped regime. It shows a C_2 symmetry with gap maxima along the (π,π) direction, rotated by 45° from the nematicity along $(0,\pi)$ or $(\pi,0)$ direction as widely discussed in the normal state.[16–48] Moreover, we also find the (π,π)-type nematicity in the under-doped and optimally doped hole-type $Ba_{1-y}K_yFe_2As_2$, with $y = 0.2$, 0.25 and 0.5. Taking these together, we suggest that the (π,π) nematic superconducting order is a universal feature in iron-based superconductors.

Methods. $BaFe_{2-x}Ni_xAs_2$ single crystals were grown by the FeAs self-flux method.[76] To enhance the resistance and hence the measurement sensitivity, we fabricated the crystals into micro bridges [Fig. 1(c)] with processes described as follows: Firstly, the crystals were cleaved into ultra-thin slices, and attached onto silicon substrates with epoxy [see Figs. 1(a) and 1(b)]. Then, the slices were etched for a thickness of about 10 nm to obtain a clean surface, and deposited a gold layer with a thickness of ∼100 nm using magnetron sputtering deposition technique. Both pro-

cesses were carried out in an *in situ* micro-fabrication system (AdNaNo-Tek Ltd.) to avoid the interface oxidation or degeneration between the crystal and conducting films. The as-prepared slices were further etched into micro-bridges using micro-fabrication technique, and the sample geometry is 20 μm in length, 5 μm in width, and $<$ 100 nm in thickness. Lastly, electrodes parties of the sample [see Fig. 1(c)] were connected by using silver paste, and then the Au layer on the surface of microbridge was etched. We note that the interface between the electrode and crystal is as silver paste/Au/crystal, leading to an ideal ohmic contact with contact resistance below 1 ohm. The thickness of the sample was confirmed by an ion-beam etching method.[77] Figure 1(c) shows a typical scanning electron microscope image of the micro-bridge, where the contacts were made along the Fe–As directions, identified from the breaking steps on the single-crystal slices as shown in Figs. 1(a) and 1(b). The ultra-thin samples were pasted onto the substrate by epoxy, thus the epoxy would generate a small stress onto the crystals due to the mismatch of thermal expansion coefficient between the epoxy and crystals. Such a stress was small but played the role of detwinning the system, and allowed the C_2-symmetry behaviors to be observed.

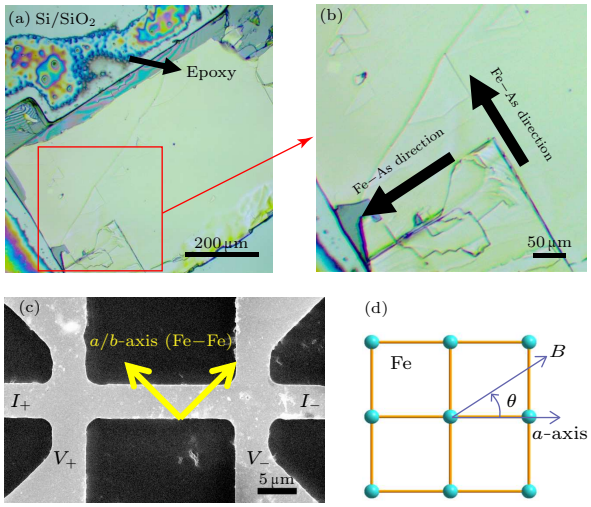

Fig. 1. Crystal and sample geometry. [(a), (b)] Optical image of the single-crystal slice. After cleaving, the straight breaking steps are along the Fe–As bonds. (c) Scanning electron microscope images for a typical ultra-thin sample in a standard Hall-bar shape. The sample is 5 μm in width, 20 μm in length, and $\sim$ 100 nm in thickness. During the measurements, the current was applied along two different lattice directions (Fe–Fe or Fe–As bonds), and for the present sample, it was along the Fe–As bonds. (d) A schematic image of the Fe-plane and the rotating angle of the magnetic fields.

The in-plane resistivity measurements were carried out in a physical properties measurement system (PPMS, Quantum Design). For each temperature, we waited for one hour for the samples to reach thermal equilibrium. Variation of the temperature due to sample rotation was verified to be less than 0.008 K. The potential misalignment of the magnetic field against the *ab*-plane was estimated to be less than 1°. For the angular-dependent resistivity measurements, the magnetic field was rotated about the *c*-axis with an angle θ as shown in the schematic image in Fig. 1(d). In all samples, the resistivity along two Fe–Fe chains were not equivalent, even for the tetragonal-structured samples, possibly due to the small strain introduced during the sample processing as discussed above. Therefore, the one along which the resistivity was smaller was defined as the *a*-axis.

The pulsed high magnetic fields experiments were performed in Wuhan National High Magnetic Field Center. The micro-bridge samples were rotated along the *c*-axis, and the magnetic field up to 50 T was applied within the *ab*-plane. The period for each field pulse is less than 10 ms, and the magnetoresistivity curves showed no hysteresis for the increasing and decreasing field processes, indicating the absence of thermal effects.

Results—Sample Characterizations. Figure 2 shows the temperature dependence of the in-plane resistivity of $BaFe_{2-x}Ni_xAs_2$ with x = 0.065, 0.075, 0.092, 0.10, 0.12, and 0.18, for which the corresponding superconducting transition temperatures are T_c = 11.48, 14.41, 18.78, 19.68, 17.61, and 5.88 K, respectively, consistent with the previous results.[76,78,79] The superconducting transition exhibits a sharp drop from the normal state, indicating the high quality of the single crystals, especially for the samples around the optimal-doped range with x = 0.092, 0.10, and 0.12, whose transition width is less than 0.5 K. For the under-doped cases with x = 0.065 and 0.075, the resistivity develops an obvious low-temperature upturn, associated with the development of the antiferromagnetic order.[78,79]

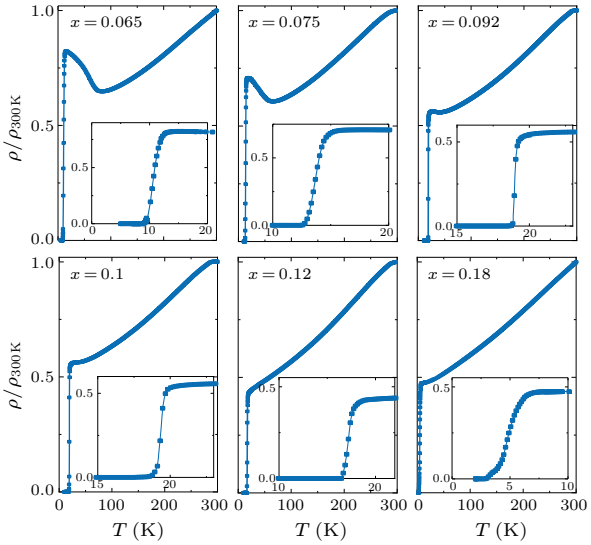

Fig. 2. Temperature dependence of the in-plane resistivity $\rho/\rho_{300\,K}$ of $BaFe_{2-x}Ni_xAs_2$ with x = 0.065, 0.075, 0.092, 0.10, 0.12, and 0.18. Inset shows the superconducting transition region.

With these high-quality single crystals covering from underdoping to overdoping, we can characterize the intrinsic transport properties of the superconductors in the whole superconducting dome. Here, in Fig. 3 we take the optimally doped $BaFe_{2-x}Ni_xAs_2$ with $x = 0.1$ as an example to illustrate the physical quantities measured and some definitions used in the following. Firstly, we measured the in-plane magnetoresistivity by rotating the *ab*-plane about the *c*-axis in a fixed magnetic field parallel to the *ab*-plane and at a fixed temperature. Figure 3(a) shows two typical curves for the angular-dependent normalized magnetoresistivity ρ/ρ_n at $T = 18$ and 19 K. Here, ρ_n corresponds to the normal-state resistivity just above T_c. The resistivity shows a clear two-fold oscillation with θ, but not the C_4 symmetry expected for the superconducting state. Since both temperatures are located at the superconducting transition region, the angular-dependent magnetoresistivity should be related to the superconductivity. However, the magnetoresistivity may have a complicated origin, such as the thermally activated vortex creep and flux flow. Therefore, we further studied directly the superconducting properties such as the angular-dependent T_c and upper critical fields (H_{c2}).

Figure 3(b) shows the temperature-dependent resistivity at the steep superconducting transition region under a magnetic field B of 9 T applied at different angles of 0, 45°, 90° and 135°. The ρ/ρ_n–T curves are considerably different with respect to the field direction, indicating that the superconductivity suppression effect of magnetic field depends on field direction. Thus, by applying external magnetic fields along different directions within the *ab*-plane, we can obtain the angular-dependent superconducting transition temperature T_c as defined in Fig. 3(b).

We also studied the angular-dependent H_{c2}, which is directly related to the superconducting gap. As demonstrated in Refs. [80–83], the anisotropic H_{c2} is an effective probe of the superconducting gap symmetry. Figure 3(c) gives the magnetoresistivity with respect to magnetic field applied in different directions. The H_{c2} as defined in Fig. 3(c) is dramatically different once applying field in different angles, being an angular-dependent H_{c2} as that of T_c.

We would like to emphasize that the central superior of the present investigation is to measure micro-scaled devices, and study the transport properties at the steep superconducting transition region. The design of micro-scaled devices can dramatically enhance the measurement signal, especially for exploring the anisotropic transport properties under external magnetic fields. As shown in Fig. 1(c), the samples have a thickness below 100 nm and width of 5 μm, by which we can enhance the resistance up to tens and hundreds of ohms to promote the sensitivity of the measurements significantly. Also, the electrodes connecting to the microbridge part is superconducting crystal, but not contacting metal onto the measured crystal directly. Therefore, thermal effects from the contact resistance in traditional samples can be basically eliminated. In the narrow superconducting transition region, the slope of the ρ–T curve is quite large. Therefore, in this region, any anisotropic behaviors with respect to the field angle can be detected sensitively.

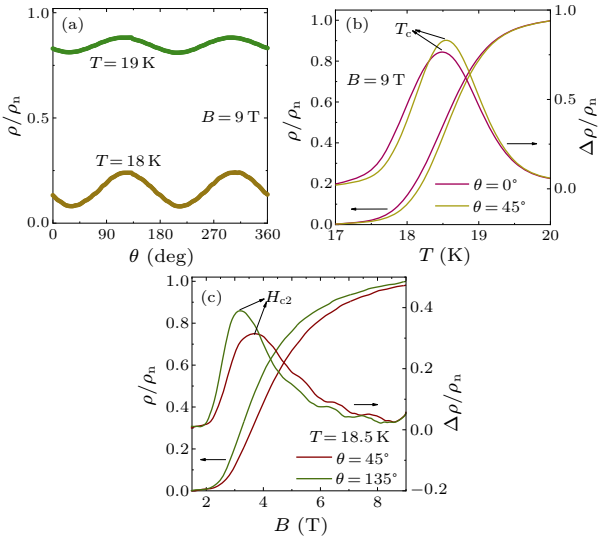

Fig. 3. Anisotropic transport property measurements on $BaFe_{1.9}Ni_{0.1}As_2$ at the steep superconducting transition region. (a) Angular dependence of the normalized in-plane magnetoresistivity at two typical temperatures of 18 and 19 K. The magnetic field was fixed at 9 T, and rotated about the *c*-axis with an angle θ as shown in the schematic image in Fig. 1(d). The ρ_n corresponds to the normal state resistivity just above the T_c. (b) Temperature dependence of the normalized resistivity under magnetic field of 9 T along typical angles of 0 and 45°. The T_c is defined as the temperature at the peak of the $\Delta\rho/\rho_n$. (c) The magnetoresistivity ρ/ρ_n as a function of magnetic field, where the field was applied in two typical angles of 45° and 135°. The magnetic field at the peak of the $\Delta\rho/\rho_n$ is defined as the upper critical field H_{c2}.

Angular-Dependent Magnetoresistivity. Based on the method described in Fig. 3(a), the angular dependence of magnetoresistivity in $BaFe_{2-x}Ni_xAs_2$ were studied in details within the whole superconducting range with doping levels of $x = 0.065$, 0.075, 0.092, 0.10, 0.12, and 0.18. These results, normalized to the normal-state resistivity ρ_n, are shown in Fig. 4. As shown in Figs. 4(g)–4(l), near offset of T_c, one can observe clear oscillations of the magnetoresistivity with θ for all the samples. Such oscillation appears at the onset of T_c, becomes more prominent as the temperature is lowered around the middle of transition, and gets weaker again toward the offset of T_c as the resistivity is getting close to zero. Despite some subtle differences of the patterns for different doping levels, a remarkable common feature of these results is that the magnetoresistivity exhibits a major C_2 symmetry, and the maximum and minimum located around 135° (315°) and 45° (225°) directions, respectively. It should be emphasized that the magnetoresistivity results in the

normal state are observed as an angular-independent behavior for all samples.

Such a C_2 symmetry is most prominent in the heavily overdoped sample with $x = 0.18$, as shown in Figs. 4(f) and 4(l). Since this sample does not undergo a structural transition, the C_4 symmetry breaking should be of electronic origin. Similar electronic nematicity with a C_4 symmetry breaking has been observed in the normal state in the under-doped and optimally doped samples of Fe-pnictide superconductors.[16–48] However, the normal-state nematicity is along the Fe–Fe direction,[16–48] or $(\pi, 0)$ in the reciprocal space, while the ordering direction found in the superconducting state in the present work is along the Fe–As direction, or (π, π). Hereafter, we term this C_2 symmetry as (π, π)-type nematicity, where the anisotropic factor is up to −16% to 15% for the minima and maxima of the magnetoresistivity, respectively. Such anisotropic factors are dramatically larger than those induced by the structural distortion in the under-doped samples, which is normally around 0.1% between the a and b axes,[16–18] but in the same order of magnitude as that induced by the $(0, \pi)/(\pi, 0)$ nematicity in the normal state.[16–48]

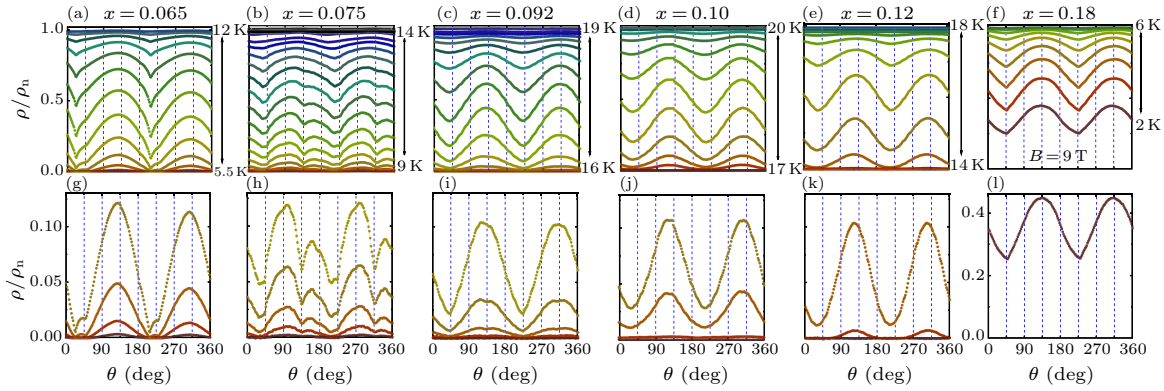

Fig. 4. (a)–(f) Angular dependence of the normalized magnetoresistivity for under- to over-doped $BaFe_{2-x}Ni_xAs_2$ with $x = 0.065$, 0.075, 0.092, 0.10, 0.12, and 0.18, measured at a series of temperatures ranging from the offset to the onset of T_c. (g)–(l) The enlarged view of the results at temperatures in the vicinity of offset-T_c. Here, the magnetic field was fixed at 9 T.

As the doping level is decreased, the maximum (minimum) deviates from 135° (45°) in the samples with $x = 0.12$, 0.10 and 0.092, and the pattern becomes more complicated in the under-doped samples with $x = 0.075$ and 0.065. For the under-doped sample with $x = 0.065$, the minima of the angular dependence of the in-plane magnetoresistivity shown in Fig. 4(a) are at $\theta \approx 23°$ and 208°, which are shifted from both the Fe–As (45° and 225°) and Fe–Fe (0 and 180°) directions. We believe that this shift is due to the superposition of the (π, π) and $(\pi, 0)$ anisotropy, the latter of which is expected to be strong in the under-doped samples.[16–48] Indeed, in the samples with $x = 0.092$, 0.10, and 0.12, although the $(\pi, 0)$ anisotropy is still present, its effect is weakened with doping. Eventually, when the doping increases to $x = 0.18$ [see Figs. 4(f) and 4(l)], this effect disappears, and the system exhibits a pure (π, π) anisotropy with the maximum and minimum of the in-plane magnetoresistivity at $\theta = 45°$ and 135°, respectively.

As for $x = 0.075$, although the in-plane magnetoresistivity follows the C_2 symmetry near the onset-T_c, a more complex pattern is observed near the offset-T_c [Figs. 4(b) and 4(h)]. In particular, while the maxima show a C_2-symmetric pattern, the minima appear to have a C_4 symmetry. However, by comparing the magnitudes of the minima, the C_2-symmetric pattern is still preserved. Moreover, the C_2-symmetric magnetoresistivity near the offset-T_c exhibits maxima around 90° and 270°, instead of around 45° and 225° as observed in other doping levels. One of the possible origins of this complex pattern at low temperatures is the quantum critical fluctuations associated with the nematic quantum critical point in this system.[31,35,41,45]

Anisotropic Superconductivity. Although the anisotropic magnetoresistivity discussed above can reflect the anisotropic superconducting properties, the interpretation may be complicated by the normal-state transport and vortex. As T_c is related to the superconducting gap directly, we studied the angular dependence of T_c for all the samples. To obtain the $T_c(\theta)$, we measured R–T curves in details by applying fields along different directions. The results are plotted as polar images shown in Figs. 5(a)–5(f), where the polar angle and radius represent the field direction and temperature, respectively. The white region illustrates 1/2 of the normal-state resistivity, which can basically tell the direction and extent of the superconducting anisotropy. The patterns of the white region are elliptical shapes for the samples [see Figs. 5(a)–5(f)], indicating a major C_2 symmetry similar to the angular-dependent magnetoresistivity results shown. For the under-doped samples ($x = 0.075$), however,

an diamond-like shape pattern can be observed in Fig. 5(b), which corresponds to a weak C_4 symmetry, consistent with the magnetoresistivity data.

From the temperature dependence of the magnetoresistivity, we can extract the T_c as illustrated in Fig. 3(b). In Figs. 5(g)–5(l), we plot $T_c(\theta)$ obtained from measurements at different angles for all the samples. For comparison purpose, we normalized T_c by $T_{c\text{-max}}$. Here, $T_{c\text{-max}}$ correspond to the maximum T_c. The $T_c/T_{c\text{-max}}(\theta)$ curves of all samples reveal a C_2 symmetry, while the occurrence of maximum and minimum are at slightly different angles, but close to 45° and 135°, respectively, consistent with the angular-dependent magnetoresistivity. For the heavily over-doped sample with $x = 0.18$, the maximum (minimum) of the $T_c/T_{c\text{-max}}$ is along the 45° (135°) direction, indicating a pure (π, π) nematicity. Since T_c is directly related to the superconducting gap, this nematicity should represent a nematic superconducting order, which is universally present in the whole superconducting dome but most prominent in the strongly under- and over-doped regimes.

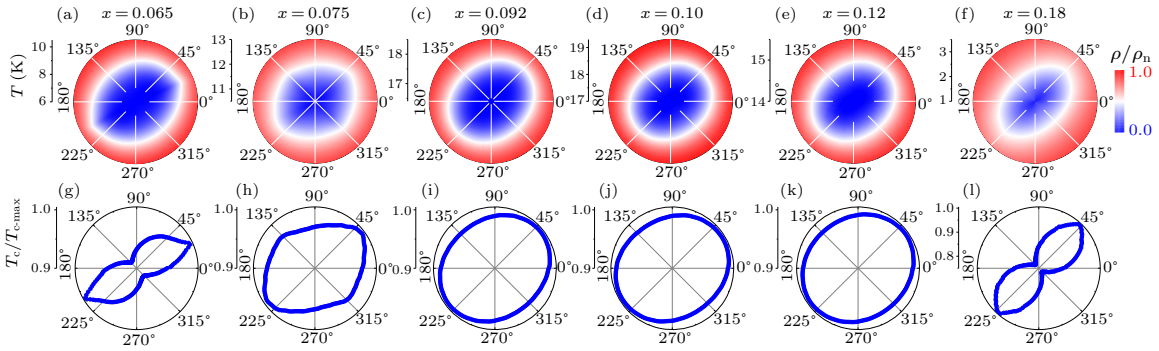

Fig. 5. (a)–(f) Polar images of temperature dependent resistivity for $BaFe_{2-x}Ni_xAs_2$ ($x = 0.065$–0.18) under magnetic fields along different directions. Here, the color bar represents ρ/ρ_n, and the magnetic field is fixed at 9 T. (g)–(l) Angular dependence of the normalized $T_c/T_{c\text{-max}}$. The T_c is estimated as the definition shown in Fig. 3(b), and $T_{c\text{-max}}$ is the maximum value. All curves demonstrate an obvious C_2 symmetry, while the under-doped sample with $x = 0.075$ demonstrates C_4 symmetry.

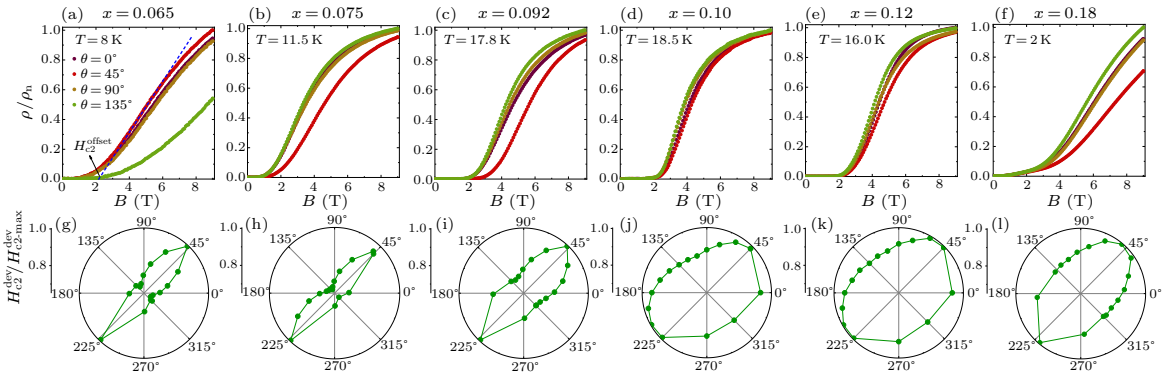

Fig. 6. (a)–(f) Magnetoresistivity ρ/ρ_n of $BaFe_{2-x}Ni_xAs_2$ ($x = 0.065$–0.18) as a function of magnetic field, where the field was applied in four typical angles of 0, 45°, 90° and 135°. (g)–(l) Angular dependence of the normalized in-plane upper critical fields $H_c/H_{c\text{-max}}(\theta)$, which is estimated as shown in Fig. 3(c).

Considering that the possible anisotropy of the pinning potential may affect the symmetry of the in-plane magnetoresistivity, we also measured the upper critical field H_{c2} to confirm that the (π, π) nematicity is an intrinsic property reflecting the nematic superconducting order, since the H_{c2} is proportional to the superconducting gap magnitude.[82,83] In Fig. 6(a)–6(f), we plot the magnetoresistivity ρ/ρ_n as a function of magnetic field for all the samples with fields applied at four typical angles of 0, 45°, 90° and 135°. Obviously, the H_{c2} as defined in Fig. 3(c) demonstrates angular-dependent behavior. Figures 6(g)–6(l) show the angular dependence of the normalized $H_{c2}/H_{c2\text{-max}}(\theta)$ for all the samples. Here, $H_{c2\text{-max}}$ represents the maximum H_{c2}. All $H_{c2}/H_{c2\text{-max}}(\theta)$ curves exhibit a C_2 symmetrical profile, with the maximum and minimum along 45° and 135°, respectively. The anisotropic $H_{c2}/H_{c2\text{-max}}(\theta)$ shares the similar behavior as the $T_c/T_{c\text{-max}}(\theta)$ results.

To compare with the above results under relatively low magnetic fields, we also applied pulsed high magnetic fields up to 50 T. Figures 7(a)–7(c) shows the ρ/ρ_n–B curves under high magnetic fields with angles ranging from 0 to 180°. The superconducting tran-

sition temperature is suppressed by about 4 K. We would like to note that all ρ/ρ_n–B curves demonstrate a clear and sharp superconducting transition, and particularly the voltage signal is unexpectedly more stable than the previous measurements on the bulk crystals.[84] The major reason is due to the improved sample quality and ultrathin device, which makes the contact resistance about one or two orders of magnitude less than that of the sample. The anisotropic H_{c2}^{onset} and H_{c2}^{offset} [see Figs. 7(d) and 7(e)] also exhibit a typical C_2 symmetry along the (π,π) direction, consistent with the data measured under low magnetic fields [see Fig. 6(p)]. Therefore, the (π,π) nematic superconductivity should be an intrinsic property independent of the field strength.

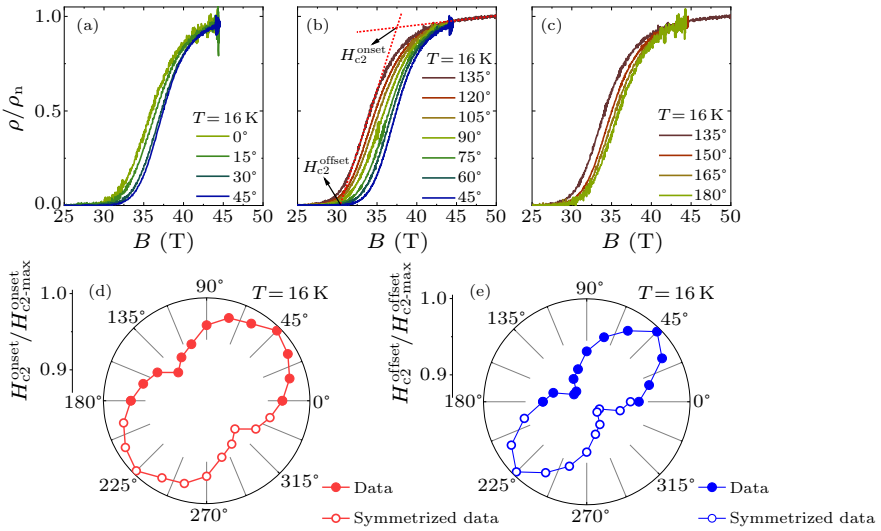

Fig. 7. Pulsed high magnetic field measurements on the optimally doped sample $BaFe_{2-x}Ni_xAs_2$ with $x = 0.10$. (a)–(c) The magnetoresistivity with respect of pulsed magnetic field up to 50 T. Here the temperature was fixed at 16 K, 4 K lower than the T_c (20 K). To avoid overlapping, the ρ/ρ_n–B curves are separated into three individual figures for angle regions 0–45°, 45°–135°, and 135°–180°, respectively. [(d), (e)] Angular dependence of $H_{c2}^{onset}/H_{c2\text{-max}}^{onset}$ and $H_{c2}^{offset}/H_{c2\text{-max}}^{offset}$ estimated from (a)–(c). Here, the hollow symbol corresponds to the symmetrized data from the measured results which are given in solid symbol.

Discussion—Ruling out Extrinsic Effects. As demonstrated above, we have found that the magnetoresistivity, superconducting critical temperatures, and upper critical fields demonstrate anisotropic profile along (π,π) directions with respect to applied magnetic fields. A natural question is whether this nematic superconductivity is caused by extrinsic factors in the experimental process. In the following, we will show that such a possibility is very low.

First, since we focus on the transport properties within the superconducting transition region, the vortex motion may contribute to the nematicity. Considering that the field is applied within the ab-plane, the vortex will flow along the c-axis, which should not induce nematic superconducting behavior within the ab-plane. Also, the anisotropic H_{c2} should be independent of the pinning potential. Thus, the vortex motion can hardly contribute to the anisotropic H_{c2}.

One may also wonder whether a symmetry-breaking field might be brought into our samples, which causes the nematic behaviors. Emphatically, we have comprehensively proven in Ref. [68] that the temperature oscillation, angle disorientation, and sample geometry can be basically ruled out by additional experiments. In addition, since the samples are in the Hall-bar geometry [see Fig. 1(c)], a C_2 oscillation as $|\sin\varphi|$ from the Lorentz force may contribute to the asymmetrical behavior, where φ represents the angle between $\boldsymbol{B}$ and $\boldsymbol{I}$. We clarify this problem by switching current flowing directions between Fe–Fe and Fe–As bonds. It is found that the orientation of the nematic superconductivity is the same, which depends only on the intrinsic crystal axes, not the current flowing directions. Actually, our previous experiments on the Corbino-shape samples have also indicated that the sample geometry and Lorentz force effects can be eliminated.[68] Therefore, the (π,π)-nematic superconductivity reflects the intrinsically anisotropic nature of the superconducting order of the sample itself.

Hole-Doping Cases. Having established the (π,π)-nematic superconducting order in the electron-doped samples, in the following we discuss the nematic superconductivity in the hole-doped $Ba_{1-y}K_yFe_2As_2$ (y = 0.2, 0.25, and 0.5). The results of $T_c(\theta)$ are shown in Fig. 8. As we have studied before, the optimally doped sample with y =0.5 displays a C_2 symmetry, but the maximum and minimum are basically along the Fe–Fe bond, or $(0,\pi)/(\pi,0)$ direction, being about 45° rotated from those of electron-doped $BaFe_{2-x}Ni_xAs_2$ samples.[68] We also note that such

anisotropy is not aligned strictly along the $(0,\pi)/(\pi,0)$ direction, but another weak anisotropy contributes as well, indicating the contribution of (π,π) nematicity. For the under-doped samples, the nematic superconductivity mainly shows a C_2 symmetry, although a weak C_4 symmetry contributes to the anisotropy as well. Nevertheless, the major anisotropy turns to be along the (π,π) direction, which rotates 45° from the optimally doped sample. Interestingly, the nematic superconductivity of the under-doped hole-type samples is in good accordance with those of electron-type ones. Moreover, the recent discovery of nematic superconductivity in heavily over-doped AFe$_2$As$_2$ (A=Rb, Cs) also has a (π,π) symmetry.[69,70]

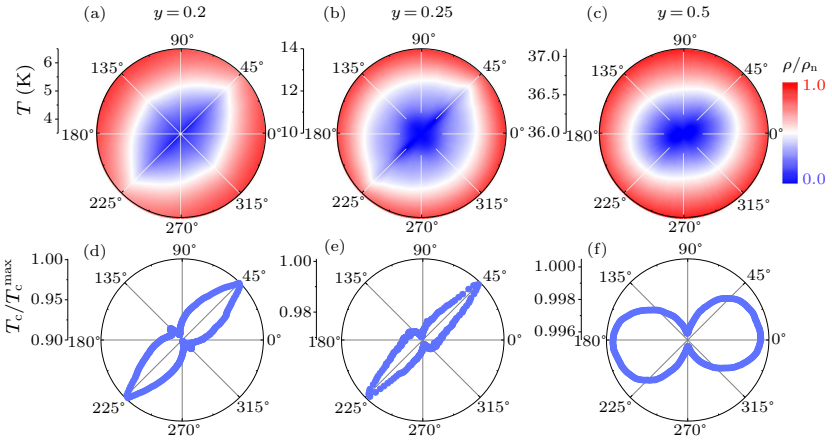

Fig. 8. Nematic superconductivity of hole-type $Ba_{1-y}K_yFe_2As_2$, with y = 0.2, 0.25 and 0.5. [(a)–(c), (d)–(f)] Angular dependence of $T_c/T_{c\text{-max}}$.

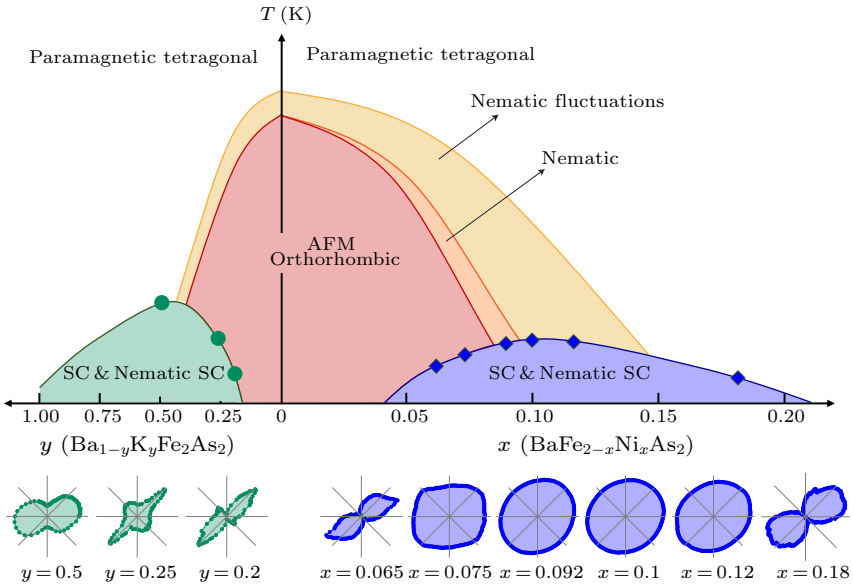

Fig. 9. Phase diagram of 122-type superconductors. Here, six samples of $BaFe_{2-x}Ni_xAs_2$ are selected ranging from under- to over-doped cases with x = 0.065, 0.075, 0.092, 0.10, 0.12, and 0.18, which are marked by blue diamond symbols. The hole-type $Ba_{1-y}K_yFe_2As_2$ results are marked as green circle symbols, and the data for the optimally doped sample with y = 0.5 are from the previous work.[68] The nematic superconductivity of AFe$_2$As$_2$ is from the scanning tunneling microscopy and elastoresistance measurements.[69,70] The yellow region demonstrates the nematic fluctuation. A narrow light orange region reveals the nematic order for the electron-doped samples. The light red region corresponds to the orthorhombic magnetism. The light blue and green areas exhibit to superconducting dome with existence of the nematic superconducting state. In the bottom, the polar plots are from the angular-dependent $T_c/T_{c\text{-max}}$ data from Figs. 5 and 8, which demonstrate the nematic superconducting order.

Phase Diagram with Nematic Superconducting Order. So far, we have unveiled the nematic superconductivity of both electron- and hole-type superconductors, and thus a phase diagram illustrating the nematic superconducting order of the 122-type Fe-based superconductors can be proposed in Fig. 9, where the polar angular-dependent $T_c/T_{c\text{-max}}$ for all the samples studied in this work is plotted. In the whole superconducting dome in $BaFe_{2-x}Ni_xAs_2$, there is a nematic superconducting order with a C_2 symme-

try along the (π,π) direction, obtained by measuring the angular dependencies of the magnetoresistivity, T_c, and H_{c2}. Such a nematic state also exists in the under-doped and optimally doped hole-type samples $Ba_{1-y}K_yFe_2As_2$, as well as the heavily hole-doped AFe_2As_2,[69,70] although the optimally doped sample has a dominant $(0,\pi)/(\pi,0)$ nematicity. These results demonstrate unambiguously the universal presence of a (π,π) nematic superconducting order in the whole superconducting dome in both the electron- and hole-doped $BaFe_2As_2$. Such nematicity is most pronounced in the heavily under- and over-doped regimes for both the electron- and hole-doped cases.

This new-type nematicity is inconsistent with the isotropic $s_\pm$-wave pairing symmetry observed previously in the optimally doped samples.[1,2,4–8] Our results cannot be explained with the d-wave pairing either, because the magnitude of the d-wave superconducting gap has a four-fold symmetry.[82,83,85] Of course, the mixing of the commonly considered $s_\pm$-wave with the rarely discussed d_{xy}-wave gap orienting along the (π,π) direction can give rise to the nematic superconducting order reported here. But since the $s_\pm$-wave and d_{xy}-wave pairings belong to different irreducible representations of the C_4 point group, they cannot be naturally mixed with each other.[49]

Possible Origin. Since the nematic superconductivity extends to the overdoped region, it is unlikely to be driven by the tetragonal-to-orthogonal structural transition, which only exists in the under-doped region as shown in Fig. 9. Moreover, even in the normal state, experiments find that the anisotropies of electronic properties in the $(\pi,0)$ nematic phase, such as the dc resistivity[17] and magnetic exchange interactions,[86] are much larger than the anisotropy of the lattice structures. On the other hand, the structural distortion breaks the equivalence between the nearest-neighbor Fe–Fe bonds, while the (π,π) nematicity breaks the equivalence between the next-nearest-neighbor Fe–Fe bonds, which correspond to the diagonals of the Fe-only square lattice. Therefore, the nematic superconductivity should not be associated with a phonon-driven structural transition, but it is more likely from an electron-driven mechanism.

For the $(\pi,0)$ nematic order, there has been increasing evidence showing that the nematicity is driven by magnetic fluctuations,[49] although the orbital scenario is also proposed.[32] In the magnetic scenario, the spin susceptibility becomes different along the $(\pi,0)$ and $(0,\pi)$ directions of the Brillouin zone before the $(\pi,0)$ magnetic order state develops. The appearance of such a nematic order is normally attributed to some quadrupole magnetic orders or fluctuations. In the orbital scenario, the occupations of the d_{xz} and d_{yz} orbits are different, which induces divergent charge fluctuations breaking the equivalence between the $(\pi,0)$ and $(0,\pi)$ directions.

Recently, some theoretical studies have been reported to explain the (π,π) nematicity in the heavily hole-doped AFe_2As_2 (A = Rb, Cs).[87–89] One of these theories is based on the itinerant picture,[87] and the origin of the nematicity is attributed to the B_{2g} bond order driven by the spin fluctuations in the d_{xy} orbits, which corresponds to the breaking of the equivalence in the next-nearest-neighbor hoppings along the two diagonals of the Fe-only square lattice. Moreover, in this scenario, the transition between the $(\pi,0)$ and (π,π) nematicities is related to the Lifshitz transition of the Fermi surface as the system goes from $y = 0.0$ to $y = 1.0$. On the other hand, a localized picture based on an extended bilinear-biquadratic Heisenberg model is proposed in Ref. [88], where the nematicity is attributed to incommensurate (q,q) magnetic fluctuations. In addition, a recent study[89] based on first-principles calculations also attributes the (π,π) nematicity to the (q,q) magnetic states, which supports symmetry-breaking composite order parameters that can condense even in the paramagnetic phase, forming the so-called vestigial phases.

Our experimental results about the (π,π) nematicity are inconsistent with the itinerant scenario, since the nematicity exists in a large doping range from heavy hole doping to heavy electron doping. In such a large doping range, the structure of the Fermi surface changes dramatically, so the (π,π) nematicity should not exist steadily in the itinerant picture. Since the orbital order normally has a strong dependence on the number of electrons, the orbital-driven mechanism of the (π,π) nematicity also seems to be inapplicable. Therefore, the magnetic-driving mechanism seems to be a more natural choice to explain our results. Because the $(\pi,0)$ and (π,π) nematicities coexist in a large doping range, the two types of nematicity are expected to originate from different degrees of freedom of the Fe $3d$ electrons and compete with each other. We note that there are many experimental evidences manifesting that the multi-orbital properties of iron-based superconductors make the electrons show both itinerancy and localization.[40,90–95] Thus, one possibility is that the $(\pi,0)$ and (π,π) nematicities come from itinerant electrons and local moments, respectively. The $(\pi,0)$ nematicity originating from the itinerant electrons has a strong doping dependence, while the (π,π) nematicity originating from the localized electrons is not sensitive to the doping concentration.

In conclusion, by performing magnetotransport measurements on ultrathin samples, we have systematically studied the angular dependence of the superconducting properties in 122-type iron-based superconductors, and found a two-fold nematic superconducting order along the (π,π) direction in the whole superconducting dome of both the electron- and hole-doped samples. This nematic order observed in the superconducting state is rotated by 45° from the $(\pi,0)$ nematicity intensively discussed in the normal state. Our results reveal that the (π,π) nematicity is a com-

mon feature of the iron-based superconductors, and constitutes as an important ingredient in the superconducting pairing mechanism.

We thank X. Dong, Z. Zhao, R. Fernandes, T. Wu, H. Yao, and H. Wen for valuable discussions and experimental supporting.

References

[1] Paglione J and Greene R L 2010 *Nat. Phys.* **6** 645
[2] Johnston D C 2010 *Adv. Phys.* **59** 803
[3] Dai P, Hu J and Dagotto E 2012 *Nat. Phys.* **8** 709
[4] Hirschfeld P J, Korshunov M M and Mazin I I 2011 *Rep. Prog. Phys.* **74** 124508
[5] Chubukov A 2012 *Annu. Rev. Condens. Matter Phys.* **3** 57
[6] Mazin I I 2010 *Nature* **464** 183
[7] Wang F and Lee D H 2011 *Science* **332** 200
[8] Norman M R 2011 *Science* **332** 196
[9] Yu S L and Li J X 2013 *Chin. Phys. B* **22** 087411
[10] Luo H, Lu X, Zhang R, Wang M, Goremychkin E A, Adroja D T, Danilkin S, Deng G, Yamani Z and Dai P 2013 *Phys. Rev. B* **88** 144516
[11] Prozorov R, Kończykowski M, Tanatar M A, Wen H H, Fernandes R M and Canfield P C 2019 *npj Quantum Mater.* **4** 34
[12] Zhao J, Rotundu C R, Marty K, Matsuda M, Zhao Y, Setty C, Bourret-Courchesne E, Hu J and Birgeneau R J 2013 *Phys. Rev. Lett.* **110** 147003
[13] Cai Y, Xie T, Yang H, Wu D, Huang J, Hong W, Cao L, Liu C, Li C, Xu Y, Gao Q, Miao T, Liu G, Li S, Huang L, Luo H, Xu Z, Gao H, Zhao L and Zhou X J 2021 *Chin. Phys. Lett.* **38** 057404
[14] Liang Y, Wu X X and Hu J P 2015 *Chin. Phys. Lett.* **32** 117402
[15] Liu S, Yuan J, Ma S, Lu Z, Zhang Y, Ma M, Zhang H, Jin K, Yu L, Zhou F, Dong X and Zhao Z 2021 *Chin. Phys. Lett.* **38** 087401
[16] Chuang T M, Allan M P, Lee J, Xie Y, Ni N, Bud'ko S L, Boebinger G S, Canfield P C and Davis J C 2010 *Science* **327** 181
[17] Chu J H, Analytis J G, De Greve K, McMahon P L, Islam Z, Yamamoto Y and Fisher I R 2010 *Science* **329** 824
[18] Song C L, Wang Y L, Cheng P, Jiang Y P, Li W, Zhang T, Li Z, He K, Wang L L, Jia J F, Hung H H, Wu C J, Ma X C, Chen X and Xue Q K 2011 *Science* **332** 1410
[19] Fisher I R, Degiorgi L and Shen Z X 2011 *Rep. Prog. Phys.* **74** 124506
[20] Chu J H, Kuo H H, Analytis J G and Fisher I R 2012 *Science* **337** 710
[21] Kuo H H, Chu J H, Palmstrom J C, Kivelson S A and Fisher I R 2016 *Science* **352** 958
[22] Liu Z, Gu Y, Zhang W, Gong D, Zhang W, Xie T, Lu X, Ma X, Zhang X, Zhang R, Zhu J, Ren C, Shan L, Qiu X, Dai P, Yang Y F, Luo H and Li S 2016 *Phys. Rev. Lett.* **117** 157002
[23] Tanatar M A, Bohmer A E, Timmons E I, Schutt M, Drachuck G, Taufour V, Kothapalli K, Kreyssig A, Bud'ko S L, Canfield P C, Fernandes R M and Prozorov R 2016 *Phys. Rev. Lett.* **117** 127001
[24] Gastiasoro M N, Paul I, Wang Y, Hirschfeld P J and Andersen B M 2014 *Phys. Rev. Lett.* **113** 127001
[25] Ying J J, Wang X F, Wu T, Xiang Z J, Liu R H, Yan Y J, Wang A F, Zhang M, Ye G J, Cheng P, Hu J P and Chen X H 2011 *Phys. Rev. Lett.* **107** 067001
[26] Allan M P, Chuang T M, Massee F, Xie Y, Ni N, Bud'ko S L, Boebinger G S, Wang Q, Dessau D S, Canfield P C, Golden M S and Davis J C 2013 *Nat. Phys.* **9** 220
[27] Sprau P O, Kostin A, Kreisel A, Bohmer A E, Taufour V, Canfield P C, Mukherjee S, Hirschfeld P J, Andersen B M and Davis J C S 2017 *Science* **357** 76
[28] Hanaguri T, Iwaya K, Kohsaka Y, Machida T, Watashige T, Kasahara S, Shibauchi T and Matsuda Y 2018 *Sci. Adv.* **4** eaar6419
[29] Singh U R, White S C, Schmaus S, Tsurkan V, Loidl A, Deisenhofer J and Wahl P 2015 *Sci. Adv.* **1** e1500206
[30] Fu M, Torchetti D A, Imai T, Ning F L, Yan J Q and Sefat A S 2012 *Phys. Rev. Lett.* **109** 247001
[31] Zhou R, Li Z, Yang J, Sun D L, Lin C T and Zheng G Q 2013 *Nat. Commun.* **4** 2265
[32] Baek S H, Efremov D V, Ok J M, Kim J S, van den Brink J and Büchner B 2015 *Nat. Mater.* **14** 210
[33] Baek S H, Bhoi D, Nam W, Lee B, Efremov D V, Büchner B and Kim K H 2018 *Nat. Commun.* **9** 2139
[34] Man H R, Guo J G, Zhang R, Schonemann R, Yin Z P, Fu M X, Stone M B, Huang Q Z, Song Y, Wang W Y, Singh D J, Lochner F, Hickel T, Eremin I, Harriger L, Lynn J W, Broholm C, Balicas L, Si Q M and Dai P C 2017 *npj Quantum Mater.* **2** 14
[35] Lu X Y, Park J T, Zhang R, Luo H Q, Nevidomskyy A H, Si Q M and Dai P C 2014 *Science* **345** 657
[36] Wang Q S, Shen Y, Pan B Y, Hao Y Q, Ma M W, Zhou F, Steffens P, Schmalzl K, Forrest T R, Abdel-Hafiez M, Chen X J, Chareev D A, Vasiliev A N, Bourges P, Sidis Y, Cao H B and Zhao J 2016 *Nat. Mater.* **15** 159
[37] Wang W Y, Song Y, Cao C D, Tseng K F, Keller T, Li Y, Harriger L W, Tian W, Chi S X, Yu R, Nevidomskyy A H and Dai P C 2018 *Nat. Commun.* **9** 3128
[38] Dai P 2015 *Rev. Mod. Phys.* **87** 855
[39] Yi M, Lu D H, Chu J H, Analytis J G, Sorini A P, Kemper A F, Moritz B, Mo S K, Moore R G, Hashimoto M, Lee W S, Hussain Z, Devereaux T P, Fisher I R and Shen Z X 2011 *Proc. Natl. Acad. Sci. USA* **108** 6878
[40] Yi M, Lu D H, Yu R, Riggs S C, Chu J H, Lv B, Liu Z K, Lu M, Cui Y T, Hashimoto M, Mo S K, Hussain Z, Chu C W, Fisher I R, Si Q and Shen Z X 2013 *Phys. Rev. Lett.* **110** 067003
[41] Liu D, Li C, Huang J, Lei B, Wang L, Wu X, Shen B, Gao Q, Zhang Y, Liu X, Hu Y, Xu Y, Liang A, Liu J, Ai P, Zhao L, He S, Yu L, Liu G, Mao Y, Dong X, Jia X, Zhang F, Zhang S, Yang F, Wang Z, Peng Q, Shi Y, Hu J, Xiang T, Chen X, Xu Z, Chen C and Zhou X J 2018 *Phys. Rev. X* **8** 031033
[42] Hashimoto T, Ota Y, Yamamoto H Q, Suzuki Y, Shimojima T, Watanabe S, Chen C, Kasahara S, Matsuda Y, Shibauchi T, Okazaki K and Shin S 2018 *Nat. Commun.* **9** 282
[43] Nakayama K, Miyata Y, Phan G N, Sato T, Tanabe Y, Urata T, Tanigaki K and Takahashi T 2014 *Phys. Rev. Lett.* **113** 237001
[44] Kretzschmar F, Bohm T, Karahasanovic U, Muschler B, Baum A, Jost D, Schmalian J, Caprara S, Grilli M, Di Castro C, Analytis J G, Chu J H, Fisher I R and Hackl R 2016 *Nat. Phys.* **12** 560
[45] Gallais Y, Paul I, Chauvière L and Schmalian J 2016 *Phys. Rev. Lett.* **116** 017001
[46] Gallais Y, Fernandes R M, Paul I, Chauvière L, Yang Y X, Méasson M A, Cazayous M, Sacuto A, Colson D and Forget A 2013 *Phys. Rev. Lett.* **111** 267001
[47] Massat P, Quan Y, Grasset R, Méasson M A, Cazayous M, Sacuto A, Karlsson S, Strobel P, Toulemonde P, Yin Z and Gallais Y 2018 *Phys. Rev. Lett.* **121** 077001
[48] Ren X, Duan L, Hu Y, Li J, Zhang R, Luo H, Dai P and Li Y 2015 *Phys. Rev. Lett.* **115** 197002
[49] Fernandes R M, Chubukov A V and Schmalian J 2014 *Nat. Phys.* **10** 97
[50] Kasahara S, Shi H J, Hashimoto K, Tonegawa S, Mizukami Y, Shibauchi T, Sugimoto K, Fukuda T, Terashima T, Nevidomskyy A H and Matsuda Y 2012 *Nature* **486** 382
[51] Davis J C and Hirschfeld P J 2014 *Nat. Phys.* **10** 184
[52] Yu R, Zhu J X and Si Q M 2018 *Phys. Rev. Lett.* **121** 227003
[53] Benfatto L, Valenzuela B and Fanfarillo L 2018 *npj Quantum Mater.* **3** 56
[54] Fernandes R M and Millis A J 2013 *Phys. Rev. Lett.* **111**

127001
[55] Kang J, Chubukov A V and Fernandes R M 2018 *Phys. Rev. B* **98** 064508
[56] Frandsen B A, Taddei K M, Yi M, Frano A, Guguchia Z, Yu R, Si Q M, Bugaris D E, Stadel R, Osborn R, Rosenkranz S, Chmaissem O and Birgeneau R J 2017 *Phys. Rev. Lett.* **119** 187001
[57] Fu L 2016 *Nat. Phys.* **12** 822
[58] Liu M, Harriger L W, Luo H, Wang M, Ewings R A, Guidi T, Park H, Haule K, Kotliar G, Hayden S M and Dai P 2012 *Nat. Phys.* **8** 376
[59] Böhmer A E, Hardy F, Wang L, Wolf T, Schweiss P and Meingast C 2015 *Nat. Commun.* **6** 7911
[60] Chubukov A V, Khodas M and Fernandes R M 2016 *Phys. Rev. X* **6** 6
[61] Mazin I I, Singh D J, Johannes M D and Du M H 2008 *Phys. Rev. Lett.* **101** 057003
[62] Kuroki K, Onari S, Arita R, Usui H, Tanaka Y, Kontani H and Aoki H 2008 *Phys. Rev. Lett.* **101** 087004
[63] Graser S, Maier T A, Hirschfeld P J and Scalapino D J 2009 *New J. Phys.* **11** 025016
[64] Yao Z J, Li J X and Wang Z D 2009 *New J. Phys.* **11** 025009
[65] Onari S and Kontani H 2012 *Phys. Rev. Lett.* **109** 137001
[66] Maiwald J, Mazin I I and Gegenwart P 2018 *Phys. Rev. X* **8** 011011
[67] Boettcher I and Herbut I F 2018 *Phys. Rev. Lett.* **120** 057002
[68] Li J, Pereira P J, Yuan J, Lv Y Y, Jiang M P, Lu D C, Lin Z Q, Liu Y J, Wang J F, Li L, Ke X X, Van Tendeloo G, Li M Y, Feng H L, Hatano T, Wang H B, Wu P H, Yamaura K, Takayama-Muromachi E, Vanacken J, Chibotaru L F and Moshchalkov V V 2017 *Nat. Commun.* **8** 1880
[69] Liu X, Tao R, Ren M Q, Chen W, Yao Q, Wolf T, Yan Y J, Zhang T and Feng D L 2019 *Nat. Commun.* **10** 1039
[70] Ishida K, Tsujii M, Hosoi S, Mizukami Y, Ishida S, Iyo A, Eisaki H, Wolf T, Grube K, Loeneysen H V, Fernandes R M and Shibauchi T 2020 *Proc. Natl. Acad. Sci. USA* **117** 6424
[71] Bao W, Qiu Y, Huang Q, Green M A, Zajdel P, Fitzsimmons M R, Zhernenkov M, Chang S, Fang M, Qian B, Vehstedt E K, Yang J, Pham H M, Spinu L and Mao Z Q 2009 *Phys. Rev. Lett.* **102** 247001
[72] Li S, de la C C, Huang Q, Chen Y, Lynn J W, Hu J, Huang Y L, Hsu F C, Yeh K W, Wu M K and Dai P 2009 *Phys. Rev. B* **79** 054503
[73] Okazaki K, Ota Y, Kotani Y, Malaeb W, Ishida Y, Shimojima T, Kiss T, Watanabe S, Chen C T, Kihou K, Lee C H, Iyo A, Eisaki H, Saito T, Fukazawa H, Kohori Y, Hashimoto K, Shibauchi T, Matsuda Y, Ikeda H, Miyahara H, Arita R, Chainani A and Shin S 2012 *Science* **337** 1314
[74] Sato T, Nakayama K, Sekiba Y, Richard P, Xu Y M, Souma S, Takahashi T, Chen G F, Luo J L, Wang N L and Ding H 2009 *Phys. Rev. Lett.* **103** 047002
[75] Yoshida T, Nishi I, Fujimori A, Yi M, Moore R G, Lu D H, Shen Z X, Kihou K, Shirage P M, Kito H, Lee C H, Iyo A, Eisaki H and Harima H 2011 *J. Phys. Chem. Solids* **72** 465
[76] Abdel-Hafiez M, Zhang Y, He Z, Zhao J, Bergmann C, Krellner C, Duan C G, Lu X, Luo H, Dai P and Chen X J 2015 *Phys. Rev. B* **91** 024510
[77] Li J, Yuan J, Yuan Y H, Ge J Y, Li M Y, Feng H L, Pereira P J, Ishii A, Hatano T, Silhanek A V, Chibotaru L F, Vanacken J, Yamaura K, Wang H B, Takayama-Muromachi E and Moshchalkov V V 2013 *Appl. Phys. Lett.* **103** 062603
[78] Ni N, Thaler A, Yan J Q, Kracher A, Colombier E, Bud'ko S L, Canfield P C and Hannahs S T 2010 *Phys. Rev. B* **82** 024519
[79] Canfield P C, Bud'ko S L, Ni N, Yan J Q and Kracher A 2009 *Phys. Rev. B* **80** 060501
[80] Mao Z Q, Maeno Y, NishiZaki S, Akima T and Ishiguro T 1985 *Sov. Phys. JETP* **62** 800
[81] Agterberg D F 1998 *Phys. Rev. Lett.* **80** 5184
[82] Mao Z Q, Maeno Y, NishiZaki S, Akima T and Ishiguro T 2000 *Phys. Rev. Lett.* **84** 991
[83] Koike Y, Takabayashi T, Noji T, Nishizaki T and Kobayashi N 1996 *Phys. Rev. B* **54** R776
[84] Yuan H Q, Singleton J, Balakirev F F, Baily S A, Chen G F, Luo J L and Wang N L 2009 *Nature* **457** 565
[85] Wu J, Bollinger A T, He X and Bozovic I 2017 *Nature* **547** 432
[86] Zhao J, Adroja D T, Yao D X, Bewley R, Li S, Wang X F, Wu G, Chen X H, Hu J and Dai P 2009 *Nat. Phys.* **5** 555
[87] Onari S and Kontani H 2019 *Phys. Rev. B* **100** 020507
[88] Wang Y, Hu W, Yu R and Si Q 2019 *Phys. Rev. B* **100** 100502
[89] Borisov V, Fernandes R M and Valentí R 2019 *Phys. Rev. Lett.* **123** 146402
[90] Xu Z, Wen J, Xu G, Chi S, Ku W, Gu G and Tranquada J M 2011 *Phys. Rev. B* **84** 052506
[91] Gretarsson H, Lupascu A, Kim J, Casa D, Gog T, Wu W, Julian S R, Xu Z J, Wen J S, Gu G D, Yuan R H, Chen Z G, Wang N L, Khim S, Kim K H, Ishikado M, Jarrige I, Shamoto S, Chu J H, Fisher I R and Kim Y J 2011 *Phys. Rev. B* **84** 100509
[92] Wang Z T, Hu W J and Nevidomskyy A H 2016 *Phys. Rev. Lett.* **116** 247203
[93] Ding X, Pan Y, Yang H and Wen H H 2014 *Phys. Rev. B* **89** 224515
[94] Glamazda A, Lemmens P, Ok J M, Kim J S and Choi K Y 2019 *Phys. Rev. B* **99** 075142
[95] Xu Z, Dai G, Li Y, Yin Z, Rong Y, Tian L, Liu P, Wang H, Xing L, Wei Y, Kajimoto R, Ikeuchi K, Abernathy D L, Wang X, Jin C, Lu X, Tan G and Dai P 2020 *npj Quantum Mater.* **5** 11